Supporting information for

Selective binding of nitrate by a neutral bis(calix[4]pyrrole) [2]rotaxane

Yifan Li [a][b], Ricardo Molina-Muriel[a], Gemma Aragay*[a] and Pablo Ballester*[a][c]

[a] *Institute of Chemical Research of Catalonia (ICIQ-CERCA), The Barcelona Institute of Science and Technology (BIST), Av. Països Catalans 16, 43007 Tarragona (Spain), E-mail: pballester@iciq.es*

[b] *Universitat Rovira i Virgili (URV), Departament de Química Analítica i Química Orgánica, c/Marcel·lí Domingo 1, 43007 Tarragona (Spain)*

[c] *ICREA, Passeig Lluís Companys 23, 08010 Barcelona (Spain)*

Corresponding Authors: P. Ballester: pballester@iciq.es; G. Aragay: garagay@iciq.es.

1. General information and instruments

Reagents were obtained from commercial suppliers and used without further purification unless otherwise stated. All solvents were commercially obtained and used without further purification except pyrrole which was distilled and freshly used. Dry solvents were either obtained from commercial suppliers or taken from a solvent system MB SPS 800 and freshly distilled. THF, Et_3N, toluene, and i-Pr_2NH were dried, distilled, and degassed by three freeze-pump-thaw cycles before being used in the cross-coupling reactions. ^1H NMR and $^{13}C\{^1H\}$ NMR spectra were recorded on a Bruker Avance 300 (300 MHz for ^1H NMR and 75 MHz for ^{13}C NMR), Bruker Avance 400 (400 MHz for ^1H NMR and 100 MHz for ^{13}C NMR), Bruker Avance 500 (500 MHz for ^1H NMR and 125 MHz for ^{13}C NMR) or Bruker Avance 500 with cryoprobe (500 MHz for ^1H NMR and 125 MHz for ^{13}C NMR). Deuterated solvents from Eurisotop are indicated in the characterization and chemical shifts are reported in ppm. 1 H NMR splitting patterns are designated as singlet (s), doublet (d), or triplet (t). Splitting patterns that could not be easily interpreted are designated as multiplet (m) or broad (br). All NMR J values are given in Hz. COSY, NOESY, ROESY, HMQC, and HMBC experiments were recorded to help with the assignment of ^1H and ^{13}C signals. Column chromatography was performed with silica gel technical grade (Sigma-Aldrich), pore size 60 Å, 230-400 mesh particle size, 40-63 μm particle size, and Thin Layer Chromatography (TLC) analysis on silica gel 60 F254

High-resolution mass spectra (HRMS) were obtained on a Bruker HPLC-TOF using ESI as ionization mode. IR spectra were recorded on a Bruker Optics FTIR Alpha spectrometer equipped with a DTGS detector, KBr beam splitter at 4 cm^{-1} resolution using a one bounce ATR accessory with diamonds windows.

^1H NMR Titrations. ^1H NMR titrations of [2]rotaxane **2** with alkylammonium salts **7a-7d** were carried out through the gradual addition of a solution of the alkylammonium salt (~10 mM) to a ~1 mM solution of [2]rotaxane **2** in the same solvent ($CDCl_3$ or $(CD_3)_2CO$) (see Supporting Information S6-S9 and S12-S15). The concentration of **2** was maintained constant throughout the titration and a ^1H NMR spectrum was registered after each addition followed by hand shacking of the NMR tube for a few seconds.

Isothermal titration calorimetry (ITC). ITC experiments were performed using a Microcal VP-ITC Microcalorimeter. HPLC grade solvents from Scharlab, SL were used. Titrations of rotaxane **2** with different alkylammonium salts in the different solvents were carried out by adding small aliquots (7-10 μL) of a solution of alkylammonium salts **7a-7d** into a solution of the host in the same solvent. The concentration of the guest was approximately 7-10 times more concentrated than the receptor solutions ([**2**] = 10^{-4} − 10^{-3} M). The apparent association constants (K_{app}), TΔS and ΔH values for the binding processes were determined from the fit of the titration data to a 1 to 1 theoretical binding model (one set of sites model implemented in Microcal software). Error values are reported as standard deviations and accurately propagated.

Computational methods. DFT calculations were performed at the RI[1,2,3]-BP86[1]-D3BJ[4,5]/def2-SVP[6,7] level of theory using Turbomole v7.0[8,9]. Calculations of ion-paired complexes (chloroform) were performed in the gas phase. Calculations of the anionic complexes (acetone) were performed both in the gas phase and using an implicit solvation model (COSMO) ($\varepsilon_{acetone}$ = 20.7, r = 3.08 Å) as implemented in Turbomole 7.0. All dataset collection of computational results of this manuscript is available in the ioChem-BD[10] repository and can be accessed through this link https://iochem-bd.iciq.es/browse/review-collection/100/69776/ccd6424184a3802e1a8c031e

2.   Synthesis and characterization of Rotaxane 2

Macrocycle **4**, pyridine N-oxide axle **5**, and stopper **6** (**Scheme S1**) were synthesized following previously reported procedures in the literature[11,12].
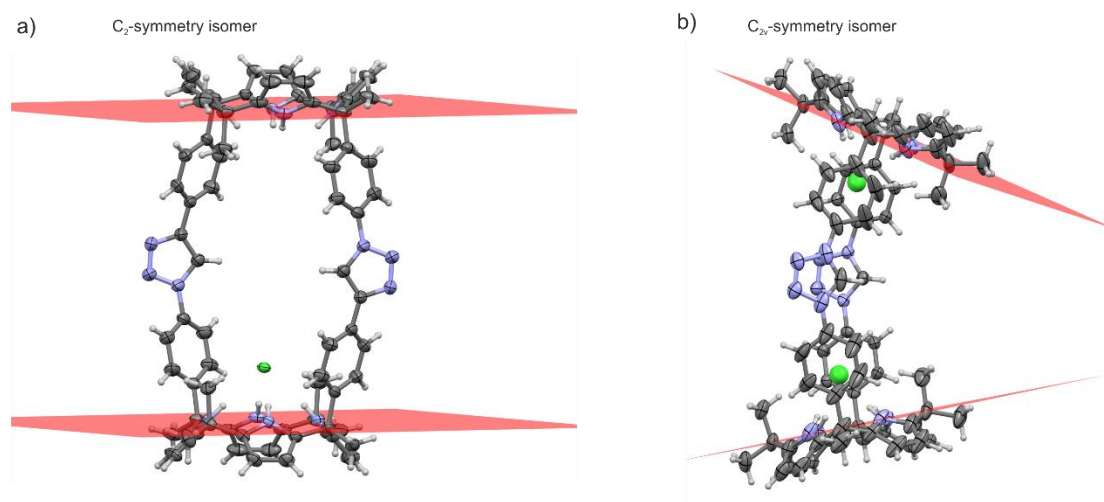

Figure S 1. X-ray structures of the 1:1 complex of macrocycle **4** with MTOA·Cl **7b** (a) and 2:1 complex of macrocycle **4** with TBA•Cl **7a** (b) reported in ref. 2. The structures show the two possible conformations that macrocycle **4** can adopt featuring C_2 and C_{2v} symmetry. Macrocycle **4**, included Cl$^-$ anions and MTOA$^+$ cation are shown as ellipsoids at 50% probability level and hydrogens as fixed-size spheres with a radius of 0.15 Å. Cations were omitted for clarity.

Rotaxane 2
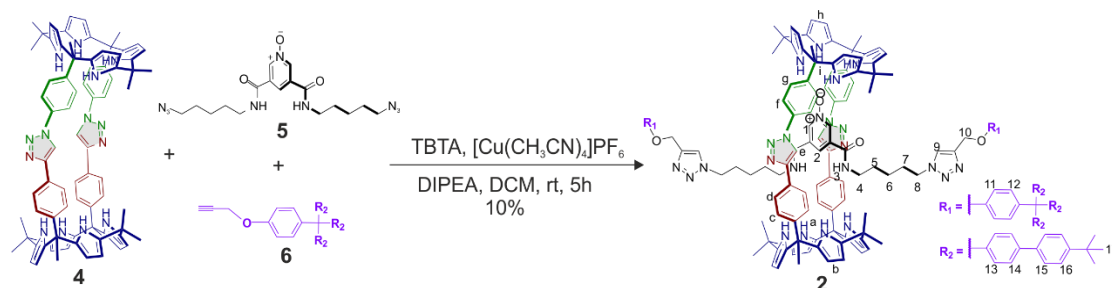
Scheme S1. Synthesis of rotaxane **2**. Reaction conditions: 1 equiv. of **4**, 2 equiv. **5** and 4 equiv. of **6**.

In a Schlenk flask, Macrocycle **4** (80.0 mg, 65.0 µmol, 1 equiv.), axle **5** (52.0 mg, 130 µmol, 2 equiv.), and stopper **6** (200 mg, 260 µmol, 4 equiv.) were dissolved in 10 mL of dry and degassed DCM under Argon atmosphere. [Cu(CH$_3$CN)$_4$]PF$_6$ (12 mg, 30 µmol, 0.5 equiv.), TBTA (17 mg, 32 µmol, 0.5 equiv.), and 0.5 mL of freshly distilled diisopropylamine were added. The reaction was stirred at room temperature for 4 h. After that, 50 mL of DCM were added to the reaction crude and the mixture was washed three times with 10 mL of water. The organic layer was dried (Na$_2$SO$_4$), filtered, and concentrated under reduced pressure to give a brown solid. The crude was purified by column chromatography on silica gel (3 g, 100:0 → 70:30 DCM:EtOAc) to afford the final product as a brown solid (20.0 mg, 13.0 µmol, 10% yield). Rf=0.4 (70:30 DCM:EtOAc).

^{1}H NMR (500 MHz, CDCl$_3$, 298 K) δ 9.15 (br, 8H, NH), 7.98 (s, 2H), 7.53 (d, 12H, J = 8.5 Hz), 7.49 (d, 12H, J = 8.5 Hz), 7.44 (d, 12H, J = 8.5 Hz), 7.39 (br, 8H), 7.29 (d, 12H, J = 8.5 Hz), 7.20 (d, 4H, J = 9.0 Hz), 7.07 (br, 8H), 6.80 (d, 4H, J = 9.0 Hz), 5.91 (m, 16H), 5.02 (br, 4H), 4.29 (br, 4H), 3.14 (br, 4H), 1.94 (br, 4H), 1.60 (br, 4H), 1.43 (br, 4H), 1.34 (s, 54 H) .^{13}C {^{1}H} NMR (125 MHz, CDCl$_3$, 298 K) δ 156.1, 150.2, 145.7, 138.4, 137.6, 137.5, 132.3, 132.1, 132.0, 131.41, 128.6, 114.3, 113.4, 67.1, 63.6, 53.5, 29.7, 29.4, 25.3, 22.3, 19.8, 14.1, 13.5, 13.4. FTIR (ATR): $\bar{\upsilon}_{max}$ (cm^{-1}) = 3443 (amine N–H stretching), 2965 (C–H stretching), 1676 (C=N stretching), 1508 (N-O stretching), 1220 (amine C–N stretching), 1039 (C=C bending), 829 (C=C bending) and 768 (C≡C bending). HR-MS (ESI-TOF-MS) m/z calculated for C$_{213}$H$_{219}$N$_{23}$O$_5$ [M − 2H]$^{-2}$ 1588.3721, found 1588.3784. mp > 190 °C (decomp).
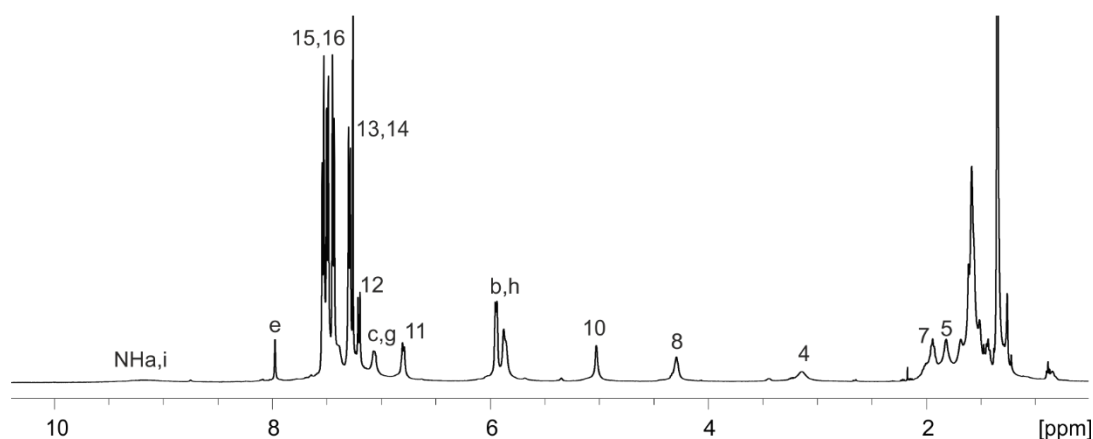

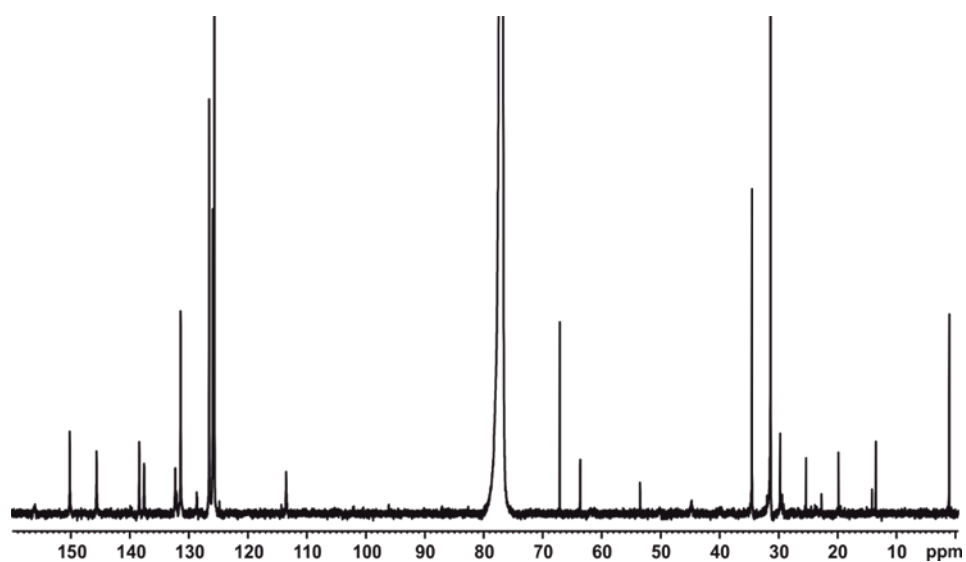**Figure S2.** ^{1}H NMR spectrum (500 MHz, 298 K, CDCl$_3$) of **2**. See Scheme S1 for proton assignment.

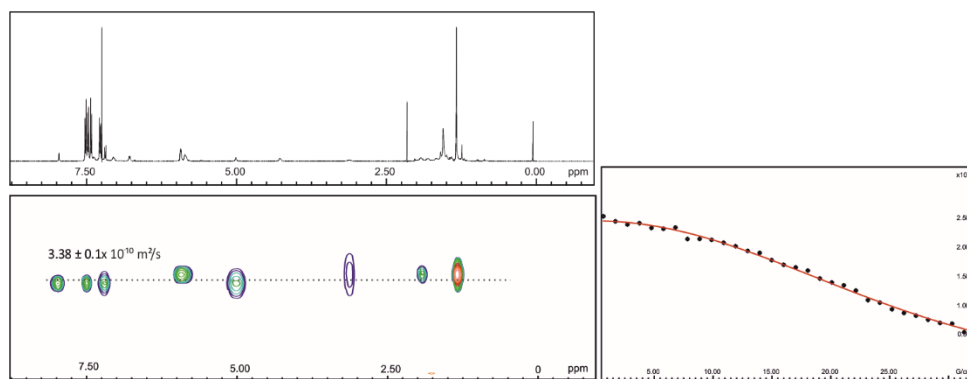**Figure S3.** ^{13}C NMR spectrum (125 MHz, 298 K, CDCl$_3$) of **2**.

Figure S4. (left) ^{1}H pseudo 2D plot of DOSY (500 MHz, 298K, CDCl$_3$) of [2]rotaxane **2** (D20 = 0.15 s, P30 = 1 ms). (right) Fit of the decay of the signal of proton He to a mono-exponential function using Dynamics Center software from Bruker. Error is indicated as standard deviation.
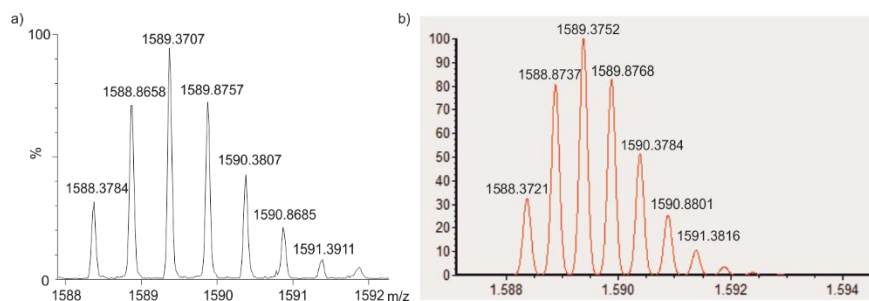

Figure S5. Experimental (a) and theoretical (b) isotopic distribution for [**2**-2H]$^{-2}$.

NO^C - Macrocycle-C$_v$ NO^N - Macrocycle-C$_v$ NO^N- Macrocycle-C$_2$ NO^C - Macrocycle-C$_2$
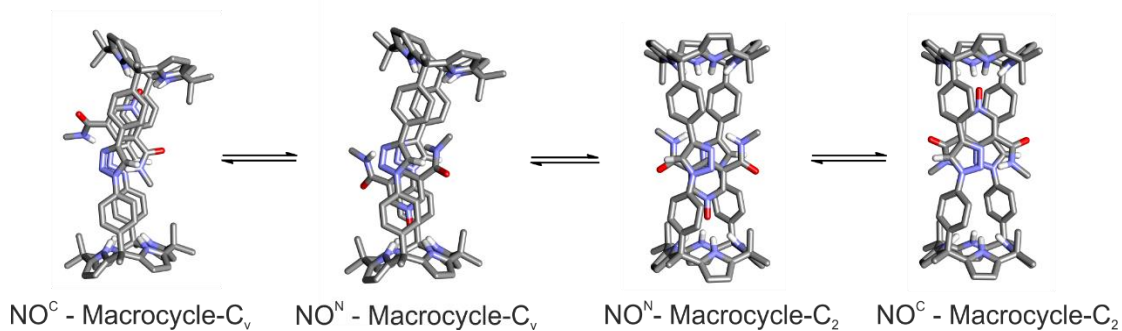
Figure S6. Equilibria between different isomers of rotaxane **2** featuring the macrocycle in two different conformations (C$_v$ and C$_2$ symmetries) and the lineal axle bound in the two chemically non-equivalent hemispheres. The alkyl chains of the axle were pruned the methyl groups for clarity.

3.   NMR experiments

3.1. CDCl₃

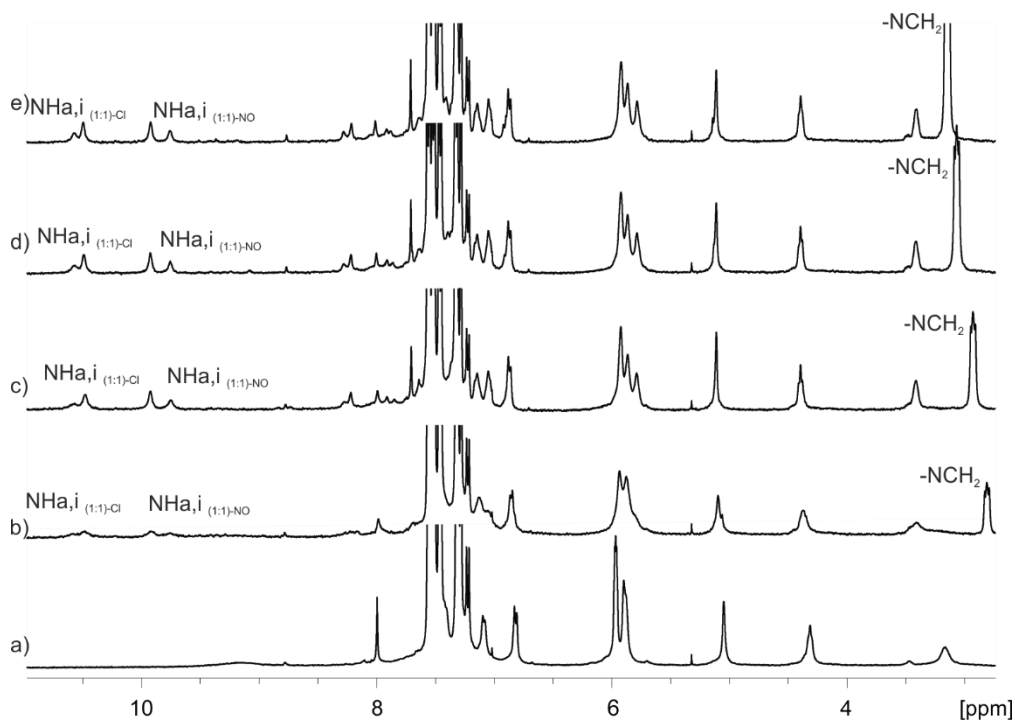### 3.1.1   NMR titration of rotaxane with TBA·Cl 7a in CDCl₃

Figure S7. Selected region of the ^{1}H NMR spectra (500 MHz, 298 K, CDCl₃) acquired during the titration experiment of **2** (a) with incremental additions of TBA·Cl **7a**, 0.5 equiv. (b), 1 equiv. (c), 1.5 equiv. (d), and 5 equiv. (e).
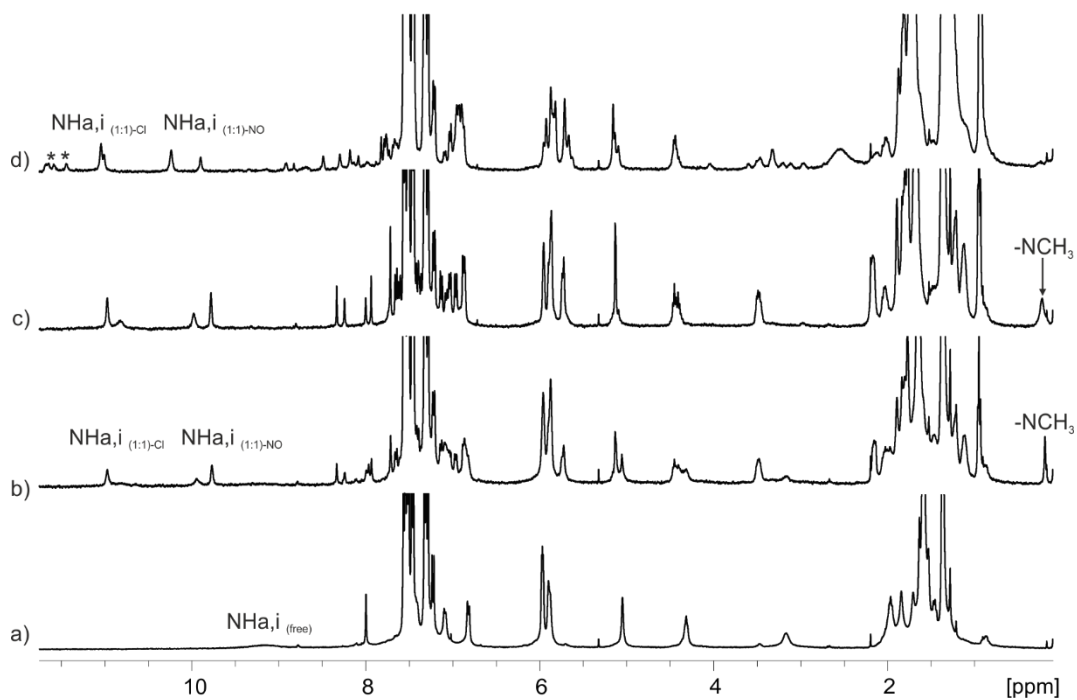
Figure S8. Selected region of the ^{1}H NMR spectra (500 MHz, 298 K, CDCl$_3$) acquired during the titration experiment of **2** (a) with incremental additions of MTOA·Cl **7b**, 0.5 equiv. (b), 1 equiv. (c) and 2 equiv. (d). * Signals related to 2:1 complex.

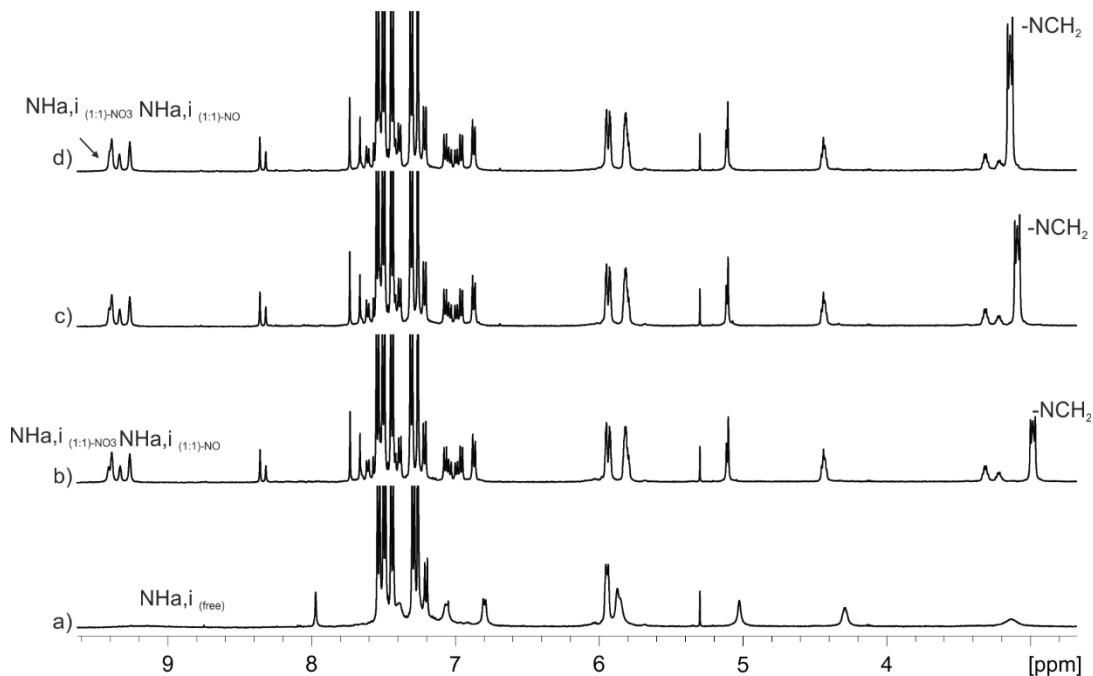### 3.1.2 NMR titration of rotaxane with TBA·NO$_3$ 7c in CDCl$_3$

Figure S9. Selected region of the ^{1}H NMR spectra (500 MHz, 298 K, CDCl$_3$) acquired during the titration experiment of **2** (a) with incremental additions of TBA·NO$_3$ **7c**, 1 equiv. (b), 1.5 equiv. (c), and 2 equiv. (d).

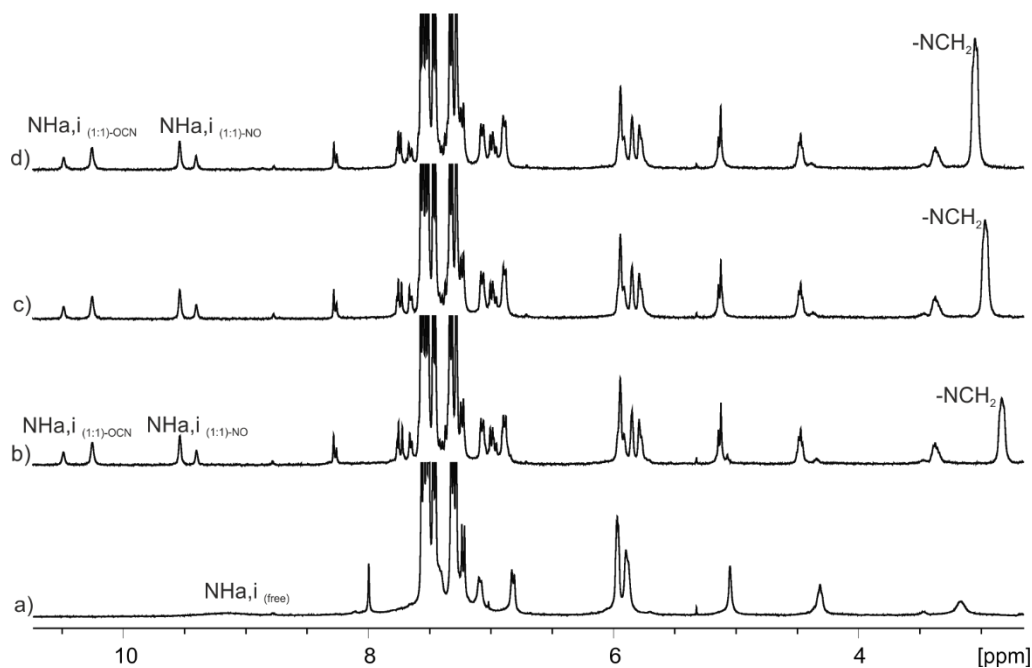### 3.1.3 NMR titration of rotaxane with TBA·OCN 7d in CDCl₃

Figure S10. Selected region of the ¹H NMR spectra (500 MHz, 298 K, CDCl₃) acquired during the titration experiment of **2** (a) with incremental additions of TBA·OCN **7d**, 1 equiv. (b), 1.5 equiv. (c), 2 equiv. (d).

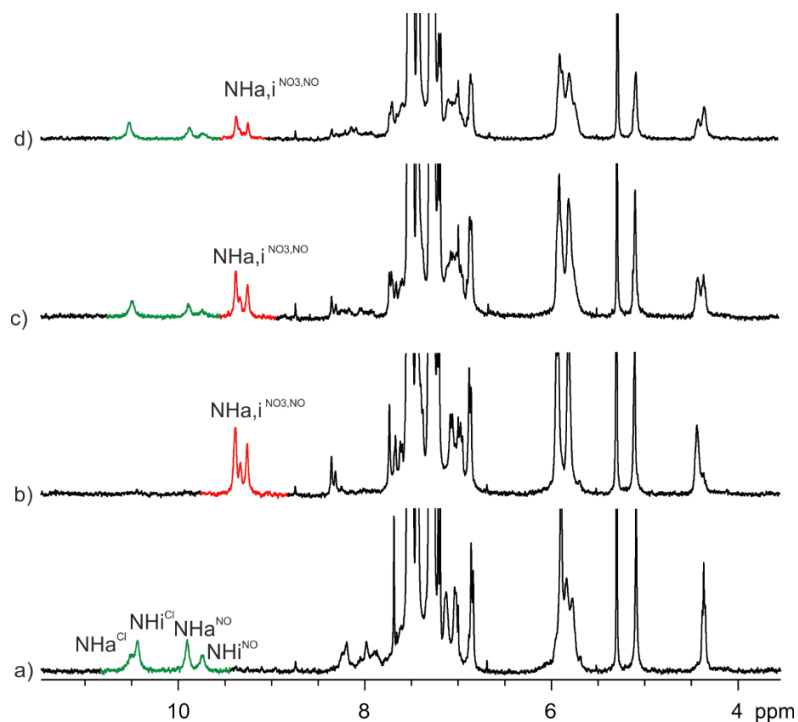### 3.1.4. Pairwise competitive experiment in CDCl₃

Figure S11. Selected region of the ¹H NMR spectra (500 MHz, 298 K, CDCl₃) acquired during the pairwise competitive experiment **2** with **7a** and **7c**. Rotaxane **2** with 1 equiv. of TBA·Cl **7a** (a), 1

equiv. of TBA·Cl **7a** and 1 equiv. of TBANO$_3$ **7c** (b), 1 equiv. of TBA·Cl **7a** and 3 equiv. of TBA·NO$_3$ **7c** (c) and 1 equiv. of TBA·Cl **7a** and 5 equiv. of TBA·NO$_3$ **7c** (d). Pyrrole NH signals of the **7a⊂2** and **7c⊂2** complexes are highlighted in green and red, respectively.
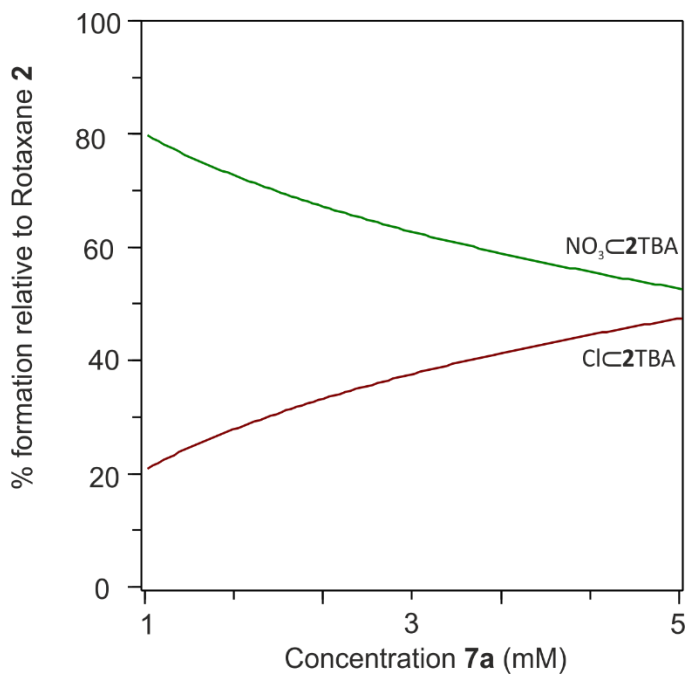

Figure S 12. Speciation profile derived using the overall concentrations of the three free components (**2**, **7a** and **7c**) used in the pair-wise experiment and the values of the association constants determined from the ITC experiments. Starting point is an equimolar solution of **2**, **7a** and **7c**.

3.2. d_6-acetone

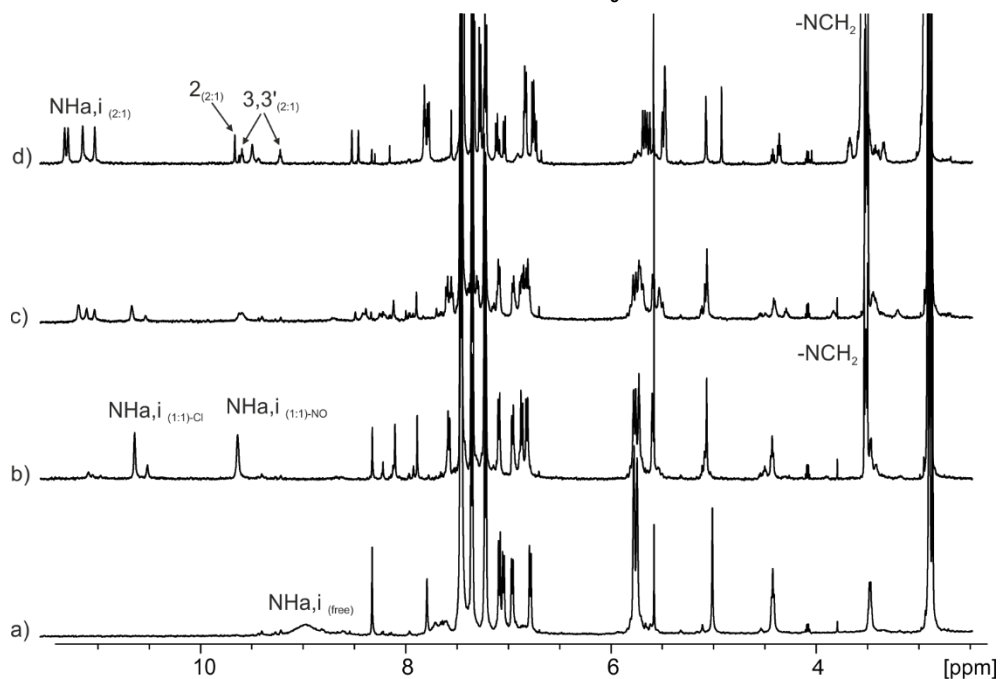#### 3.2.1. NMR titration of rotaxane with TBA·Cl 7a in d_6-acetone

Figure S13. Selected region of the ^{1}H NMR spectra (500 MHz, 298 K, d_6-acetone) acquired during the titration experiment of **2** (a) with incremental additions of TBA·Cl **7a**, 1 equiv. (b), 2 equiv. (c), and 10 equiv. (d).

3.2.2. NMR titration of rotaxane with MTOA·Cl 7b in d_6-acetone

3.2.3. NMR titration of rotaxane with TBA·NO$_3$ 7c in d_6-acetone

Figure S15. Selected region of the ^{1}H NMR spectra (500 MHz, 298 K, d_6-acetone) acquired during the titration experiment of **2** (a) with incremental additions of TBA·NO$_3$ **7c**, 1 equiv. (b), 2 equiv. (c).

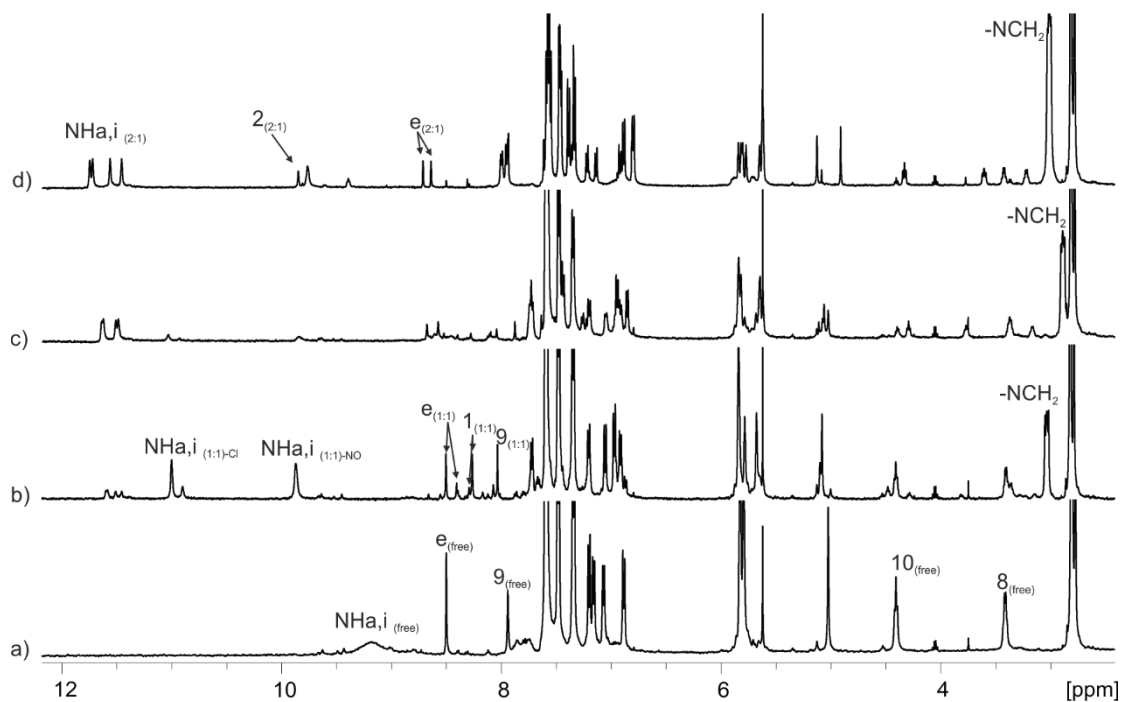**3.2.4. NMR titration of rotaxane with TBA·OCN 7d in *d₆*-acetone**
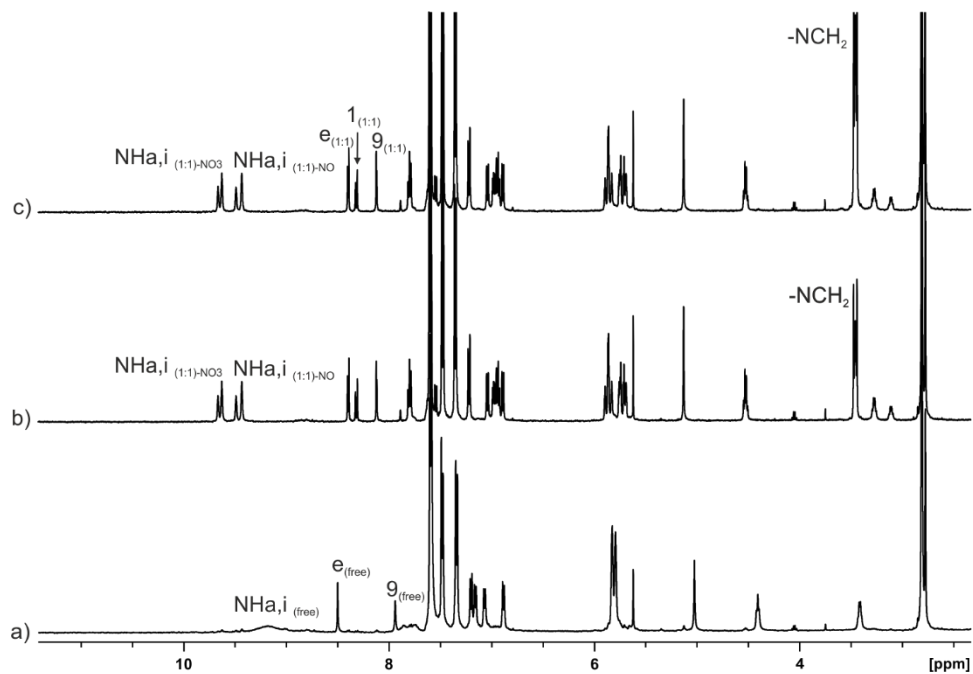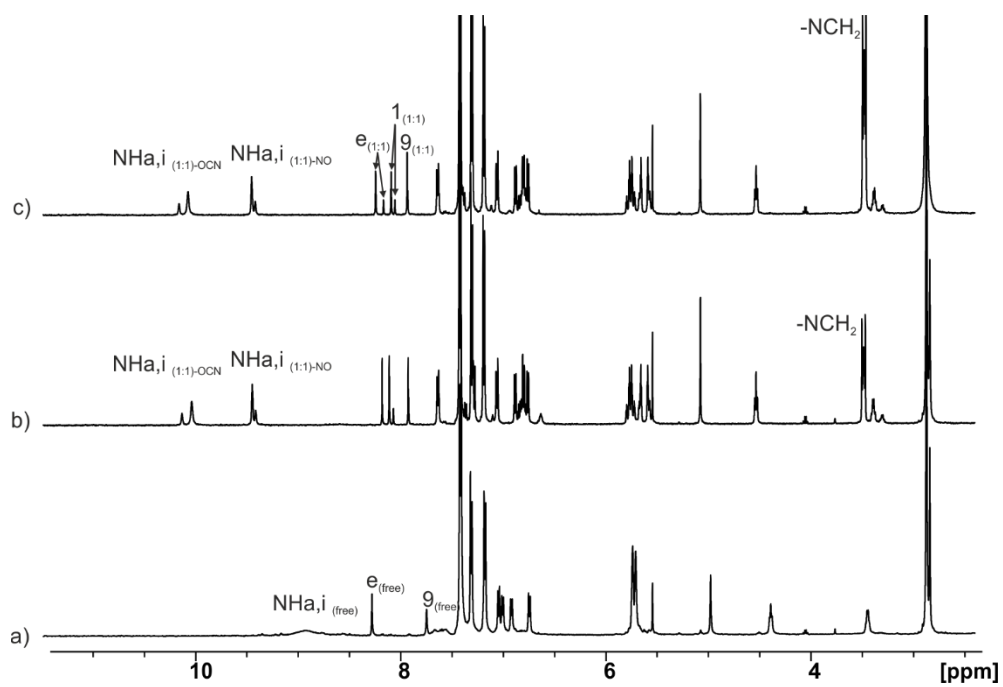

Figure S16. Selected region of the ¹H NMR spectra (500 MHz, 298 K, *d₆*-acetone) acquired during the titration experiment of **2** (a) with incremental additions of TBA·OCN **7d**, 1 equiv. (b), 2 equiv. (c).

4. ITC experiments

4.1. Chloroform

4.1.1 ITC experiments of rotaxane with TBA·Cl 7a in chloroform

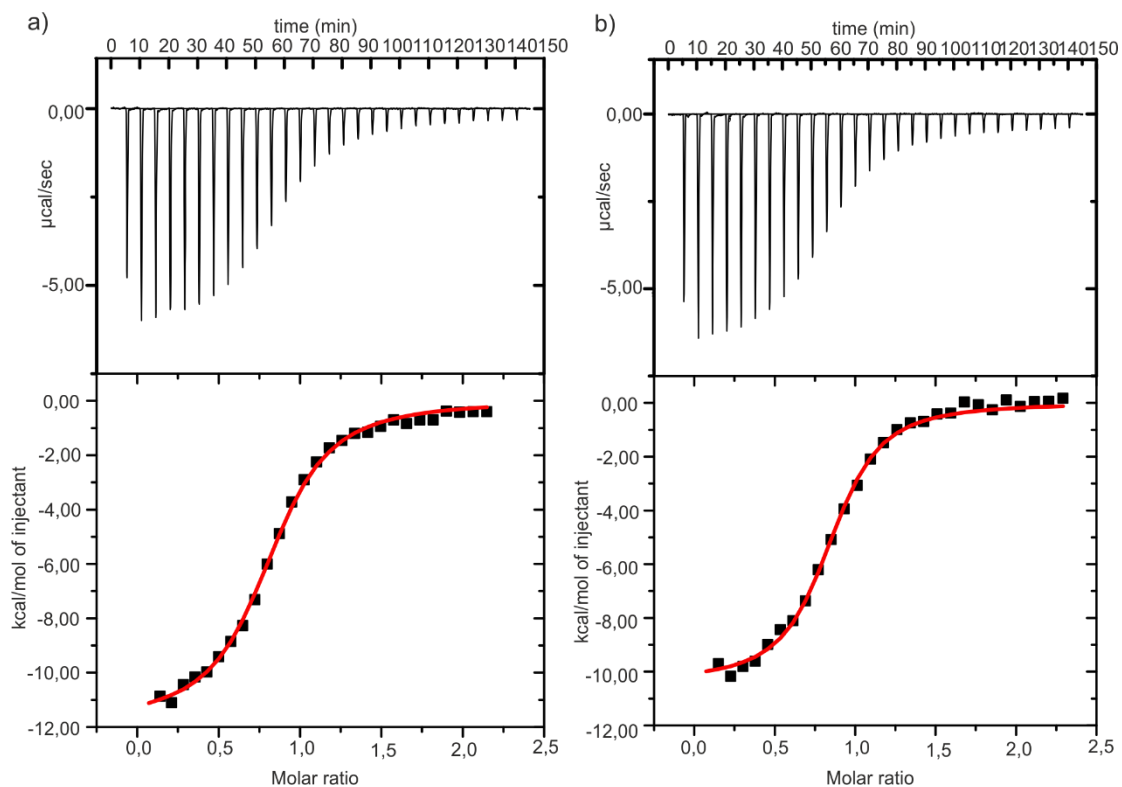**Figure S17.** Top — Traces of the raw data of the titration experiment of 1.5×10^{-4} M solution of [2]rotaxane **2**, with TBA·Cl **7a** solution 1.5×10^{-3} M (a) and 1.4×10^{-3} M (b) in chloroform. Bottom — binding isotherms of the calorimetric titration shown on top. To determine the values of the thermodynamic variables the ITC data was fitted to a 1:1 binding model (red line).

4.1.2 ITC experiment of rotaxane with MTOA•Cl 7b in chloroform

a)

b)

Figure S18. Top — Traces of the raw data of the titration experiment of 1.5×10^{-4} M (a) and 1.2×10^{-4} M (b) solution of [2]rotaxane **2**, with MTOA·Cl **7b** solution 1.2×10^{-3} M (a) and 1.0×10^{-3} M (b) in chloroform. Bottom — binding isotherms of the calorimetric titration shown on top. To determine the values of the thermodynamic variables the ITC data was fitted to a 1:1 binding model (red line).

4.1.3 ITC experiment of rotaxane with TBA·NO$_3$ 7c in chloroform

Figure S19. a **)** Top — Traces of the raw data of the titration experiment of 1.3×10^{-4} M (a) and 1.1×10^{-4} M (b) solution of [2]rotaxane **2**, with TBA·NO$_3$ **7c** solution 1.8×10^{-3} M (a) and 0.9×10^{-3} M (b) in chloroform. Bottom — binding isotherms of the calorimetric titration shown on top. To determine the values of the thermodynamic variables the ITC data was fitted to a 1:1 binding model (red line). b)

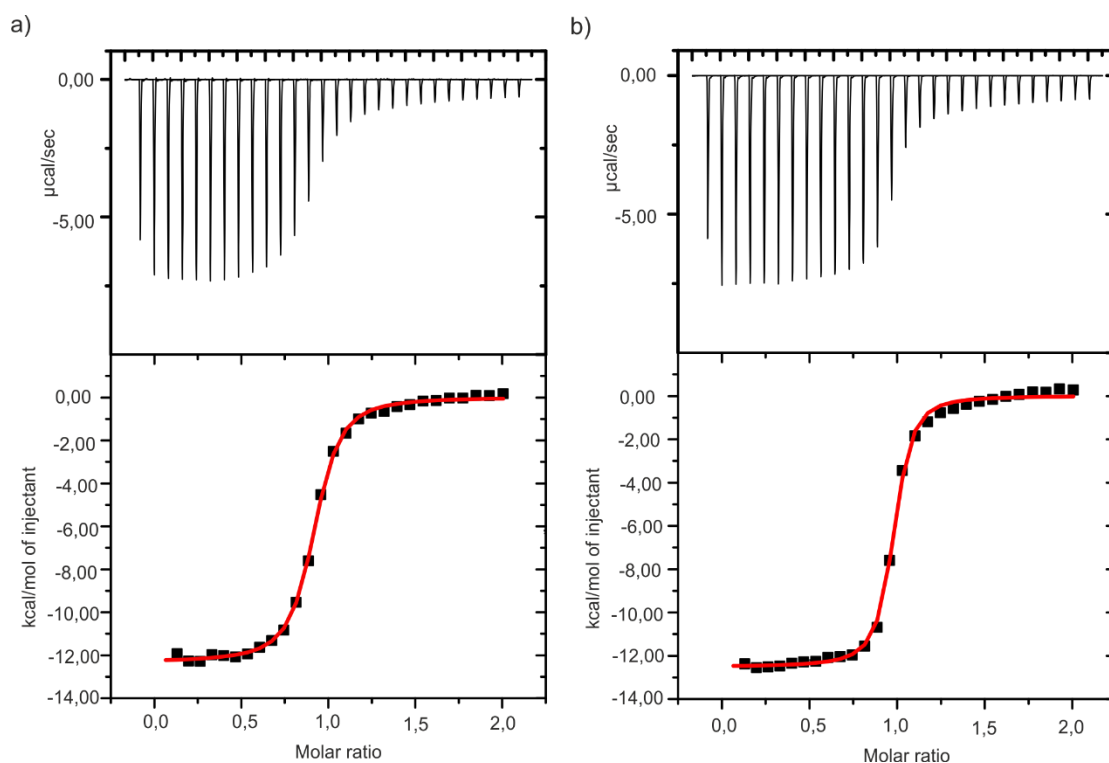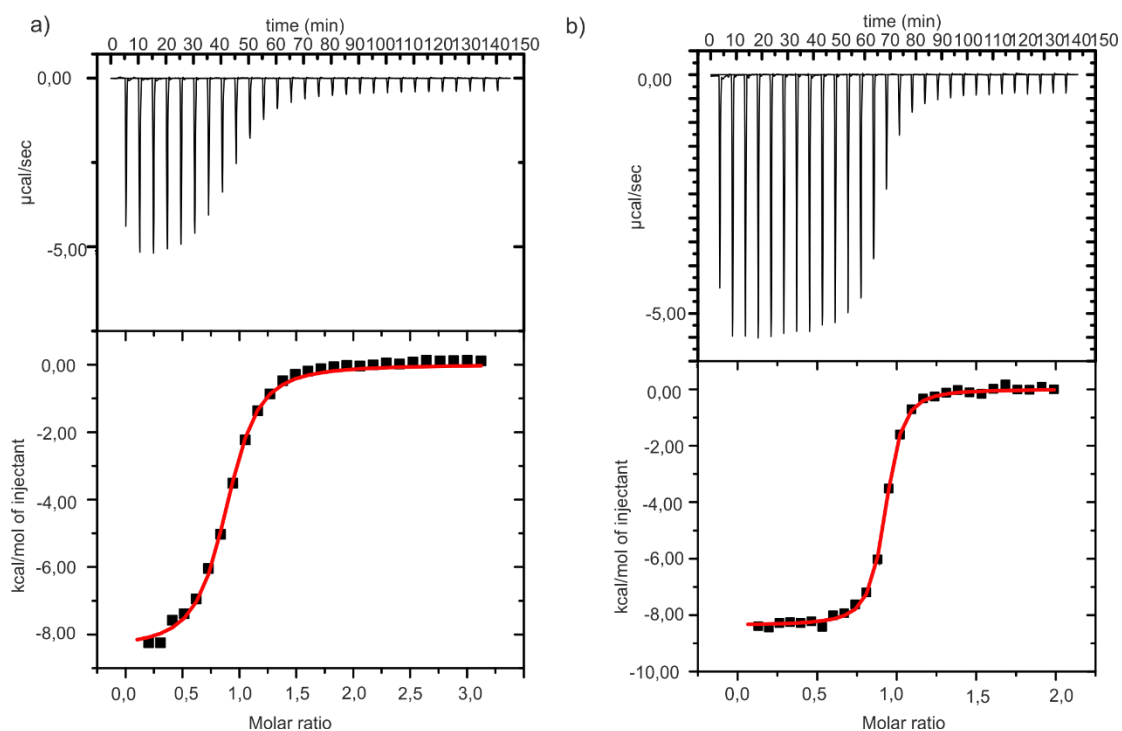### 4.1.4 ITC experiment of rotaxane with TBA·OCN 7d in chloroform

Figure S20. Top — Traces of the raw data of the titration experiment of 1.3×10^{-4} M solution of [2]rotaxane **2**, with TBA·OCN **7d** solution 1.1×10^{-3} M (a) and 1.3×10^{-3} M (b) in chloroform. Bottom — binding isotherms of the calorimetric titration shown on top. To determine the values of the thermodynamic variables the ITC data was fitted to a 1:1 binding model (red line).

4.2. Acetone

4.2.1. ITC experiment of rotaxane with TBA·Cl 7a in acetone

Figure S21. Top — Traces of the raw data of the titration experiment of 1.2×10^{-4} M solution of [2]rotaxane **2**, with TBA·Cl solution 1.1×10^{-3} M in acetone. Bottom — binding isotherms of the calorimetric titration shown on top. To determine the values of the thermodynamic variables the ITC data was fitted to a 1:1 binding model (red line).
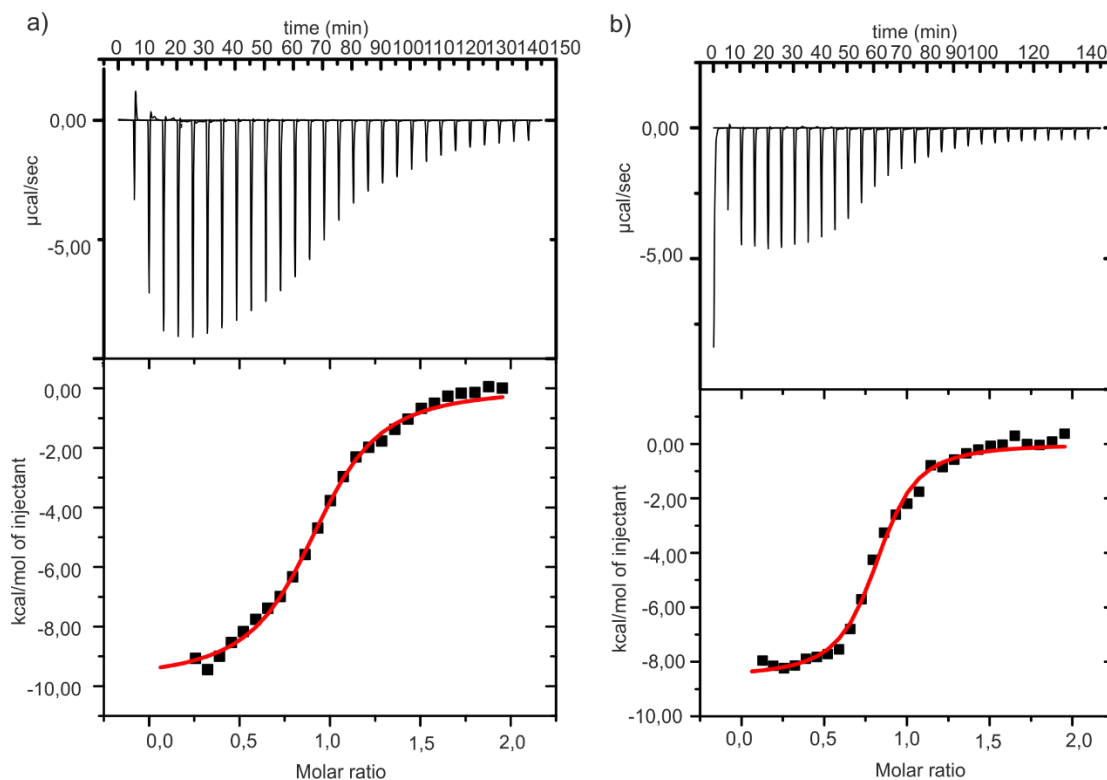
4.2.2. ITC experiment of rotaxane with TBA·NO₃ 7c in acetone

Figure S22. Top — Traces of the raw data of the titration experiment of 1.5×10^{-4} M solution of [2]rotaxane **2**, with TBA·NO₃ **7c** solution 1.2×10^{-3} M in acetone. Bottom — binding isotherms of the calorimetric titration shown on top. To determine the values of the thermodynamic variables the ITC data was fitted to a 1:1 binding model (red line).

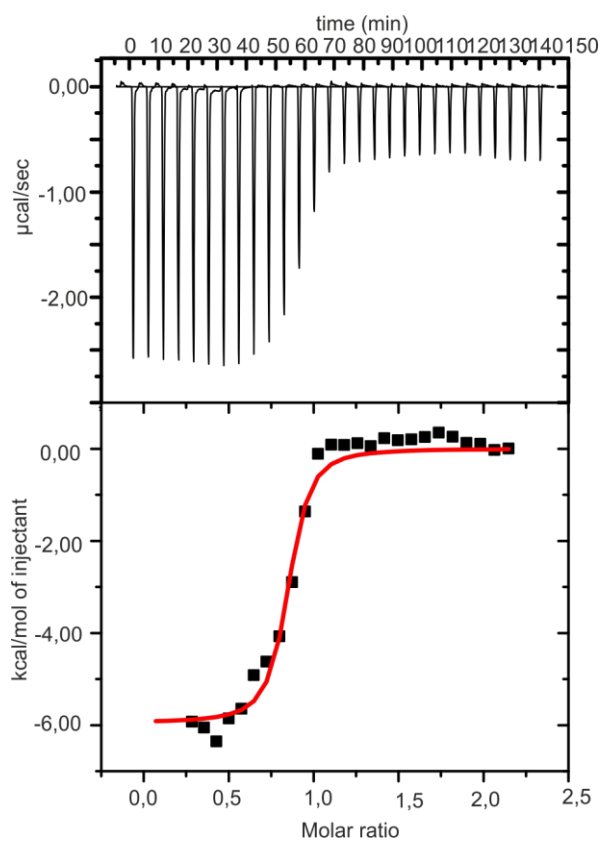### 4.2.3. ITC experiment of rotaxane with TBA·OCN 7d in acetone
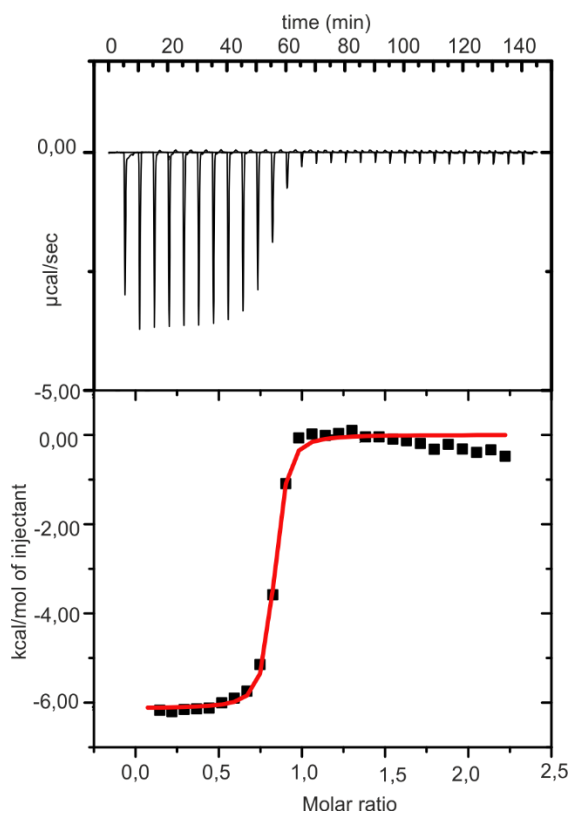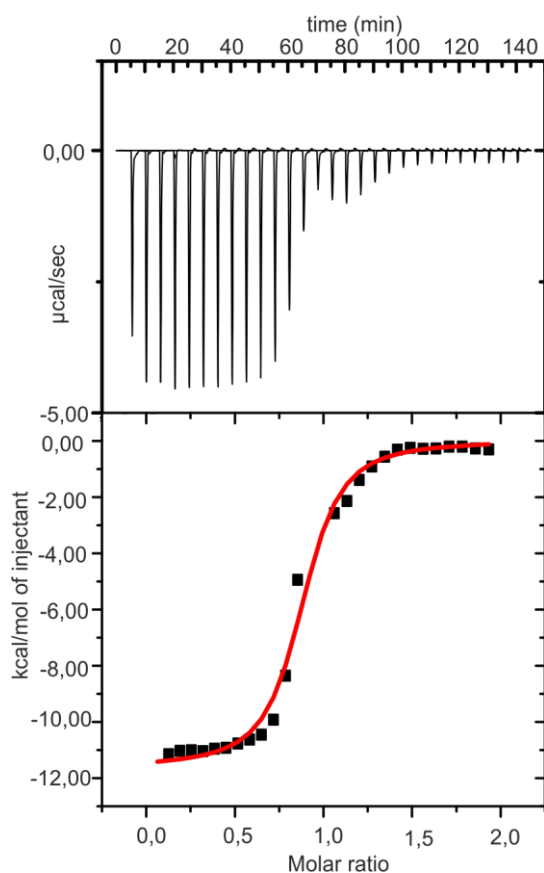

Figure S23. Top — Traces of the raw data of the titration experiment of 1.2×10^{-4} M solution of [2]rotaxane **2**, with TBA·OCN **7d** solution 1.1×10^{-3} M in acetone. Bottom — binding isotherms of the calorimetric titration shown on top. To determine the values of the thermodynamic variables the ITC data was fitted to a 1:1 binding model (red line).

5. DFT Calculations

All dataset collection of computational results of this manuscript is available in the ioChem-BD[13] repository and can be accessed through this link https://iochem-bd.iciq.es/browse/review-collection/100/69776/ccd6424184a3802e1a8c031e.

The binding equilibria considered for the calculation of the electronic energies of the binding processes tabulated in **Table S1** are depicted below.
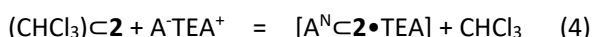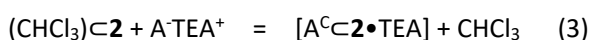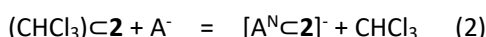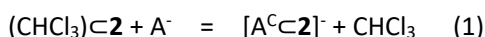
$$(CHCl_3) \subset \mathbf{2} + A^- = [A^C \subset \mathbf{2}]^- + CHCl_3 \quad (1)$$

$$(CHCl_3) \subset \mathbf{2} + A^- = [A^N \subset \mathbf{2}]^- + CHCl_3 \quad (2)$$

$$(CHCl_3) \subset \mathbf{2} + A^- TEA^+ = [A^C \subset \mathbf{2} \bullet TEA] + CHCl_3 \quad (3)$$

$$(CHCl_3) \subset \mathbf{2} + A^- TEA^+ = [A^N \subset \mathbf{2} \bullet TEA] + CHCl_3 \quad (4)$$

Table S 1. Computed electronic energies (E) of each component involved in the binding processes of equilibria 1-4 (see above) calculated using DFT calculations (gas phase) at the BP86[14]-D3BJ[15,16]/def2-SVP[17,18] level of theory using Turbomole v7.0. The electronic energy of the binding processes (ΔE), the differences in electronic energies between the complexes featuring the anion in the C-substituted or N-substituted hemisphere $\Delta E(C-N)$, and the $\Delta\Delta E$ of the binding processes of the different studied anions are depicted.

	E (kcal·mol^{-1})	ΔE (kcal·mol^{-1})	$\Delta E(C-N)$ (kcal·mol^{-1})	$\Delta\Delta E$ (A-NO$_3$) (kcal·mol^{-1})
[Cl^C⊂**2**]$^-$	**-3187371.758**	-74.5[a]	-0.2[c]	-9,8[d]
[Cl^N⊂**2**]$^-$	**-3187371.603**	-74.3[a]		-9,7[d]
[NO$_3$^{C}⊂**2**]$^-$	**-3073990.774**	-64.7[a]	-0.1[c]	0[d]
[NO$_3$^{N}⊂**2**]$^-$	**-3073990.606**	-64.6[a]		0[d]
[OCN^C⊂**2**]$^-$	**-3003323.402**	-67.0[a]	-0.1[c]	-2.3[d]
[OCN^N⊂**2**]$^-$	**-3003323.289**	-66.9[a]		-2,3[d]
[Cl^C⊂**2**•TEA]	**-3421317.213**	-52.8[b]	-4.8[d]	3.1[d]
[Cl^N⊂**2**•TEA]	**-3421312.502**	-48.0[b]		3.2[d]
[NO$_3$^{C}⊂**2**•TEA]	**-3307933.487**	-55.9[b]	-4.7[d]	0[d]
[NO$_3$^{N}⊂**2**•TEA]	**-3307928.814**	-51.2[b]		0[d]

[OCN^C⊂**2**•TEA]	**-3237267.979**	-60.7^b	-5.6	-4.8
[OCN^N⊂**2**•TEA]	**-3237262.360**	-55.1^b		-3.9^d
(CHCl$_3$)⊂**2**	**-3791381.700**	-	-	-
Cl$^-$	**-289881.375**	-	-	-
NO$_3^-$	**-176510.106**	-	-	-
OCN$^-$	**-105840.485**			
TEA•Cl	**-523848.526**			
TEA•NO$_3$	**-410461.705**			
TEA•OCN	**-339791.338**			
TEA$^+$	**-233852.837**			
CHCl$_3$	**-893965.770**			

^{a} ΔE = (E([A$^{C/N}$⊂**2**]$^-$) + E(CHCl$_3$)) − (E((CHCl$_3$)⊂**2**) + E(A$^-$)); ^{b}ΔE = (E([A$^{C/N}$⊂**2**•TEA]) + E(CHCl$_3$)).−
(E((CHCl$_3$)⊂**2**) + E(TEAA));^{c} ΔE = E([A^C⊂**2**]$^-$) - E([A^N⊂**2**]$^-$); ^{d} ΔE = E([A^C⊂**2**•TEA]) - E([NO$_3^N$⊂**2**•TEA]).

Table S 2. Computed electronic energies (E) calculated using DFT calculations using an implicit solvation model (COSMO) at the same level of theory used before in Table S1. The ΔΔE of the binding processes of the different studied anionic complexes are depicted.

	E (kcal·mol^{-1})	ΔE^a	ΔΔE^b (kcal·mol^{-1})
[Cl^C⊂**2**]$^-$	**-3187411.457**	-2897455.45	0
[NO$_3^C$⊂**2**]$^-$	**-3074029.327**	-2897455.49	-0.04
[OCN^C⊂**2**]$^-$	**-3003362.828**	-2897456.28	-0.83
Cl$^-$	**-289956.0068**		
NO$_3^-$	**-176573.8397**		
OCN$^-$	**-105906.5461**		

^{a} **ΔE** = (E([A^C⊂**2**]$^-$) - E(A$^-$)); ^{b} **ΔΔE** = ΔE([A^C⊂**2**]$^-$) − ΔE([Cl^C⊂**2**]$^-$)
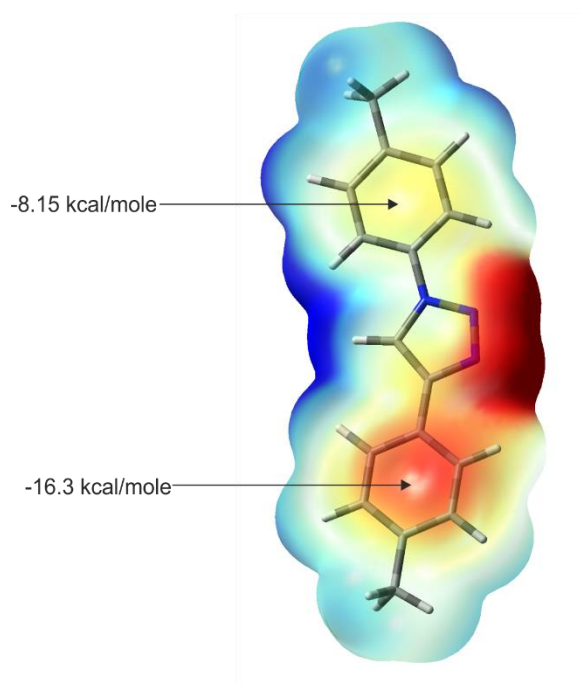
-8.15 kcal/mole

-16.3 kcal/mole

Figure S 24. Calculated ESP values for the model system of N- and C- substituted meso phenyls defining the two aromatic hemispheres of the macrocycle. ESP cubes were mapped at an electron density value of 0.001 a.u using Gaussian 09.[19]
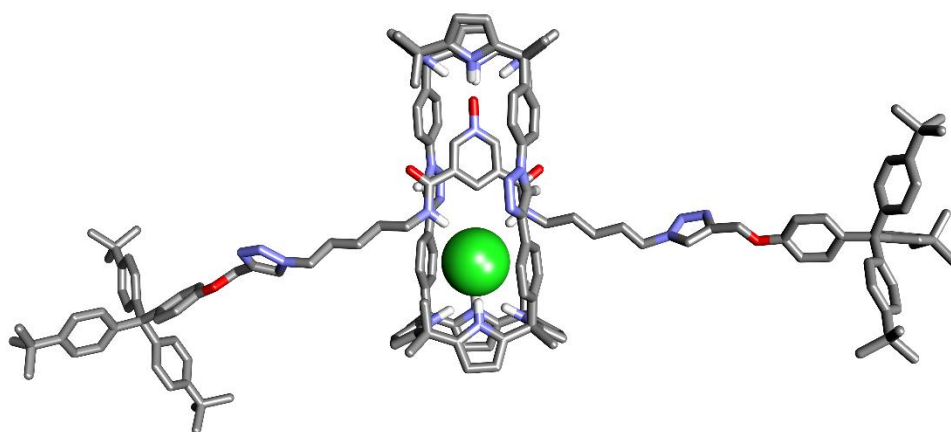

Figure S25. Energy-minimized structure of the 1:1 complex Cl⊂**2.** The macrocycle and the axle are shown in stick representation. The chloride is shown as CPK model.
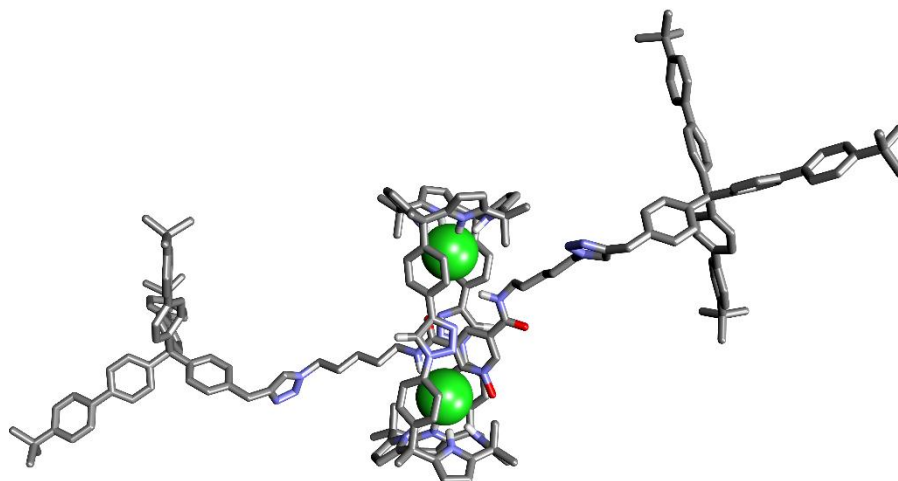
Figure S26. Energy-minimized structure of the 2:1 complex (Cl)$_2$⊂**2**. The macrocycle and the axle are shown in stick representation. The chloride is shown as CPK model.

6. References

[1] Perdew, J. P., Density-functional approximation for the correlation energy of the inhomogeneous electron gas. *Phys. Rev. B* **1986,** *33* (12), 8822-8824.

[2] Eichkorn, K.; Weigend, F.; Treutler, O.; Ahlrichs, R., Auxiliary basis sets for main row atoms and transition metals and their use to approximate Coulomb potentials. *Theor. Chem. Acc.* **1997,** *97* (1), 119-124.

[3] Sierka, M.; Hogekamp, A.; Ahlrichs, R., Fast evaluation of the Coulomb potential for electron densities using multipole accelerated resolution of identity approximation. *J. Chem. Phys.* **2003,** *118* (20), 9136-9148.

[4] Grimme, S.; Ehrlich, S.; Goerigk, L., Effect of the damping function in dispersion corrected density functional theory. *J. Comput. Chem.* **2011,** *32* (7), 1456-1465.

5 Grimme, S.; Antony, J.; Ehrlich, S.; Krieg, H., A consistent and accurate ab initio parametrization of density functional dispersion correction (DFT-D) for the 94 elements H-Pu. *J. Chem. Phys.* **2010,** *132* (15).

6 Rappoport, D.; Furche, F., Property-optimized Gaussian basis sets for molecular response calculations. *J. Chem. Phys.* **2010,** *133* (13).

7 Schäfer, A.; Horn, H.; Ahlrichs, R., Fully optimized contracted Gaussian basis sets for atoms Li to Kr. *J. Chem. Phys.* **1992,** *97* (4), 2571-2577.

8 TURBOMOLE V7.0 2015, a Development of University of Karlsruhe and Forschungszentrum Karlsruhe GmbH, 1989–2007, TURBOMOLE GmbH, Since 2007. Available online: http://www.turbomole.com

9 Ahlrichs, R.; Bär, M.; Häser, M.; Horn, H.; Kölmel, C., Electronic structure calculations on workstation computers: The program system turbomole. *Chem. Phys. Lett.* **1989,** *162* (3), 165-169.

10 M. Álvarez-Moreno, C. de Graaf, N. López, F. Maseras, J. M. Poblet and C. Bo, Managing the Computational Chemistry Big Data Problem: The ioChem-BD Platform, *Journal of Chemical Information and Modeling*, 2015, **55**, 95-103.

11 J. R. Romero, G. Aragay and P. Ballester, Ion-pair recognition by a neutral [2]rotaxane based on a bis-calix[4]pyrrole cyclic component, *Chem. Sci.*, 2017, **8**, 491-498.

12 R. Molina-Muriel, G. Aragay, E. C. Escudero-Adán and P. Ballester, Switching from Negative-Cooperativity to No-Cooperativity in the Binding of Ion-Pair Dimers by a Bis(calix[4]pyrrole) Macrocycle, *J. Org. Chem.*, 2018, **83**, 13507-13514.

13 M. Álvarez-Moreno, C. de Graaf, N. López, F. Maseras, J. M. Poblet and C. Bo, Managing the Computational Chemistry Big Data Problem: The ioChem-BD Platform, *Journal of Chemical Information and Modeling*, 2015, **55**, 95-103.

14 J. P. Perdew, Density-functional approximation for the correlation energy of the inhomogeneous electron gas, *Phys. Rev. B*, 1986, **33**, 8822-8824.

[15] S. Grimme, S. Ehrlich and L. Goerigk, Effect of the damping function in dispersion corrected density functional theory, *J. Comput. Chem.*, 2011, **32**, 1456-1465.

[16] S. Grimme, J. Antony, S. Ehrlich and H. Krieg, A consistent and accurate ab initio parametrization of density functional dispersion correction (DFT-D) for the 94 elements H-Pu, *J. Chem. Phys.*, 2010, **132**.

[17] D. Rappoport and F. Furche, Property-optimized Gaussian basis sets for molecular response calculations, *J. Chem. Phys.*, 2010, **133**.

[18] A. Schäfer, H. Horn and R. Ahlrichs, Fully optimized contracted Gaussian basis sets for atoms Li to Kr, *J. Chem. Phys.*, 1992, **97**, 2571-2577.

[19] Gaussian 09, Revision A.02, M. J. Frisch, G. W. Trucks, H. B. Schlegel, G. E. Scuseria, M. A. Robb, J. R. Cheeseman, G. Scalmani, V. Barone, B. Mennucci, G. A. Petersson, H. Nakatsuji, M. Caricato, X. Li, H. P. Hratchian, A. F. Izmaylov, J. Bloino, G. Zheng, J. L. Sonnenberg, M. Hada, M. Ehara, K. Toyota, R. Fukuda, J. Hasegawa, M. Ishida, T. Nakajima, Y. Honda, O. Kitao, H. Nakai, T. Vreven, J. A. Montgomery, Jr., J. E. Peralta, F. Ogliaro, M. Bearpark, J. J. Heyd, E. Brothers, K. N. Kudin, V. N. Staroverov, R. Kobayashi, J. Normand, K. Raghavachari, A. Rendell, J. C. Burant, S. S. Iyengar, J. Tomasi, M. Cossi, N. Rega, J. M. Millam, M. Klene, J. E. Knox, J. B. Cross, V. Bakken, C. Adamo, J. Jaramillo, R. Gomperts, R. E. Stratmann, O. Yazyev, A. J. Austin, R. Cammi, C. Pomelli, J. W. Ochterski, R. L. Martin, K. Morokuma, V. G. Zakrzewski, G. A. Voth, P. Salvador, J. J. Dannenberg, S. Dapprich, A. D. Daniels, Ö. Farkas, J. B. Foresman, J. V. Ortiz, J. Cioslowski, D. J. Fox, Gaussian, Inc. Wallingford CT, 2009.